Missouri University of Science and Technology
Scholars' Mine

Electrical and Computer Engineering Faculty Research & Creative Works

Electrical and Computer Engineering

01 Jul 2023

A Non-Line-of-Sight Mitigation Method For Indoor Ultra-Wideband Localization With Multiple Walls

Mengyao Dong

Yihong Qi
Missouri University of Science and Technology, qiyi@mst.edu

Xianbin Wang

Yiming Liu

Follow this and additional works at: https://scholarsmine.mst.edu/ele_comeng_facwork

 Part of the Electrical and Computer Engineering Commons

Recommended Citation

M. Dong et al., "A Non-Line-of-Sight Mitigation Method For Indoor Ultra-Wideband Localization With Multiple Walls," *IEEE Transactions on Industrial Informatics*, vol. 19, no. 7, pp. 8183 - 8195, Institute of Electrical and Electronics Engineers, Jul 2023.
The definitive version is available at https://doi.org/10.1109/TII.2022.3217533

This Article - Journal is brought to you for free and open access by Scholars' Mine. It has been accepted for inclusion in Electrical and Computer Engineering Faculty Research & Creative Works by an authorized administrator of Scholars' Mine. This work is protected by U. S. Copyright Law. Unauthorized use including reproduction for redistribution requires the permission of the copyright holder. For more information, please contact scholarsmine@mst.edu.

A Non-Line-of-Sight Mitigation Method for Indoor Ultra-Wideband Localization With Multiple Walls

Mengyao Dong, *Graduate Student Member, IEEE*, Yihong Qi, *Senior Member, IEEE*, Xianbin Wang, *Fellow, IEEE*, and Yiming Liu

***Abstract*—Ultra-wideband (UWB) ranging techniques can provide accurate distance measurement under line-of-sight (LOS) conditions. However, various walls and obstacles in indoor non-LOS (NLOS) environments, which obstruct the direct propagation of UWB signals, can generate significant ranging errors. Due to the complex through-wall UWB signal propagation, most conventional studies simplify the ranging error model by assuming that the incidence angle is zero or the relative permittivities for different walls are the same to improve the through-wall UWB localization performance. Considering walls are different in realistic settings, this article presents a through-multiple-wall NLOS mitigation method for UWB indoor positioning. First, spatial geometric equilibrium equations of UWB through-wall propagation and a numerical method are developed for the precise modeling of UWB through-wall ranging errors. Then, calculated error maps are determined numerically without field measurements. Finally, the determined error maps are combined with a gray wolf optimization algorithm for localization. The proposed method is evaluated via field experiments with four rooms, three walls, and six penetration cases. The results demonstrate that the method can strongly mitigate the multi-wall. NLOS effects on the performance of UWB positioning systems. This solution can reduce project costs and number of power supplies for UWB indoor positioning applications.**

***Index Terms*—Error map, gray wolf optimization (GWO), indoor localization, non-line-of-sight (NLOS), through-wall, ultra-wideband (UWB).**

Manuscript received 23 May 2022; revised 9 September 2022; accepted 9 October 2022. Date of publication 27 October 2022; date of current version 20 June 2023. This work was supported by the Sichuan Science and Technology Program under Grant 2020JDRC0030 and Grant 2019JDRC0129. Paper no. TII-22-2205. *(Corresponding author: Mengyao Dong.)*

Mengyao Dong and Yiming Liu are with the School of Information Science and Technology, Southwest Jiaotong University, Chengdu 611756, China (e-mail: dongmengyao@my.swjtu.edu.cn; liuyiming@my.swjtu.edu.cn).

Yihong Qi is with the Southwest Jiaotong University, Chengdu 611756, China, also with the Pontosense Inc., Waterloo, ON N2J 4G8, Canada, also with the Missouri University of Science and Technology, Rolla, MO 65409 USA, and also with the Western University, London, ON N6A 5B9, Canada (e-mail: yihongqi@gmail.com).

Xianbin Wang is with the Department of Electrical and Computer Engineering, Western University, London, ON N6A 5B9, Canada (e-mail: xianbin.wang@uwo.ca).

Color versions of one or more figures in this article are available at https://doi.org/10.1109/TII.2022.3217533.

Digital Object Identifier 10.1109/TII.2022.3217533

I. Introduction

In the era of Industry 4.0, indoor positioning technology has been widely used in different industrial applications such as robot services and smart manufacturing [1], [2]. The indoor positioning market will reach $41 billion by 2022 [3]. Many wireless technologies, particularly Bluetooth [4], radio frequency identification (RFID) tags [5], and Wi-Fi [2], have been utilized to achieve indoor positioning. In large-scale scenarios, Bluetooth and RFID technologies have the advantages of low cost and low power consumption [4], [5]. Wi-Fi-based systems can leverage existing Wi-Fi infrastructures without additional hardware costs [2], [6]. However, these techniques do not provide high positioning accuracy [7], and they often divide the indoor map into many grids to sample signal fingerprints, which requires high human workloads. Alternatively, ultra-wideband (UWB) technology has attracted intensive attention [1], [8], [9]. With its extremely high bandwidth, short pulse waveform, and low transmission power, UWB technology offers the advantages of high accuracy, strong penetration ability, long range, robustness to multipath, and good coexistence with other communication systems [10]. Therefore, UWB technology is a desirable solution for indoor positioning.

Using UWB technology for planar indoor positioning requires at least three UWB nodes with fixed locations as anchors around the indoor area. Another UWB mobile node, named tag, has to continuously range with the anchors to determine its changing location. The measured distances from the anchors to the tag are used as inputs to a localization algorithm to locate the mobile tag.

There may be one or multiple obstacles in the service area, e.g., movable furniture or fixed walls, between the UWB tag and anchors, leading to non-line-of-sight (NLOS) scenarios [1], [11], [12]. Ranging results based on time of arrival (TOA) may contain positive errors in excess of 1 m in NLOS scenarios, compared with the 20-cm ranging accuracy that is common in line-of-sight (LOS) cases [1], [8]. In practice, to provide high-precision indoor positioning, additional UWB anchors have to be installed on both sides of a wall to avoid NLOS ranging due to walls, which means each room is equipped with a separate positioning system. A room length is generally less than 20 m, whereas the maximum operational range of UWB can reach 100 m [10]. As a result, applications of using an independent positioning system in each room fail to take advantage of UWB technology's long-distance ranging and good

1551-3203 © 2022 IEEE. Personal use is permitted, but republication/redistribution requires IEEE permission.
See https://www.ieee.org/publications/rights/index.html for more information.

Authorized licensed use limited to: Missouri University of Science and Technology. Downloaded on August 16,2023 at 18:44:54 UTC from IEEE Xplore. Restrictions apply.

penetration. Furthermore, additional UWB anchors significantly increase UWB hardware complexity and deployment costs, which hampers the large-scale development of UWB positioning applications [13].

Many kinds of surrounding objects could induce NLOS propagation in UWB positioning and different methods have been proposed to mitigate different NLOS effects, such as walls [1], furniture [7], and human body [9]. Walls and their effects have attracted many specialized studies due to their ubiquity and immobility. Studying the UWB through-wall localization can be combined with other NLOS mitigation methods to address hybrid NLOS situations.

Among the UWB NLOS mitigation methods, map-based methods are suitable for relatively static indoor environments [7]. The map-based methods utilize the layout of the specific positioning environment and the tag position to determine the NLOS situation, i.e., the number of walls between an anchor and a tag [10]. It is possible to leverage through-wall error information to mitigate the NLOS errors. However, UWB through-wall ranging errors could be complex due to the unknown layered materials in each wall. Recently, researchers have approximated the through-wall ranging error models by assuming that the relative permittivities for different walls are the same [1], [12] or measured UWB positioning error maps [7] to improve the positioning accuracy. For example, Silva and Hancke reduced the NLOS localization errors by 42%–69% after implementing a simplified error-model-based mitigation algorithm [1]. Based on our extensive literature survey, the following three research gaps have been identified.

1) Existing UWB through-wall ranging error models are simplified and are not suitable for multiple walls.
2) Map-based UWB NLOS localization algorithms are often based on the preliminary tag position [1], which may incorrectly determine the error model used.
3) Existing fingerprint methods require a large number of time-consuming measurement points in the field.

To address the above research gaps, this article proposes an NLOS mitigation method for UWB indoor localization in the presence of multiwall obstacles. The contributions are summarized as follows.

1) We propose a numerical solution with spatial geometric equilibrium equations for the UWB through-wall ranging error model. The solution is adequate for one or multiple walls of different thicknesses and materials and thus can be applied in a wide variety of scenarios.
2) We develop a method for calculating the error map based on the proposed UWB through-wall ranging error model. The error map can be determined numerically without field measurements, which is significantly different from other measured error maps.
3) We combine the error maps with a gray wolf optimization (GWO) algorithm for positioning UWB tags and verify the method using static and continuous experiments.

The rest of this article is organized as follows. Section II reviews the existing methods. Section III introduces the UWB through-wall ranging. Section IV presents the proposed method. Section V describes experiments, results, and discussions. Finally, Section VI concludes this article.

TABLE I
RECENT EXISTING RESEARCH ON UWB NLOS MITIGATION

Ref.	Year	Category	Algorithm
[14]	2021	Channel-based	Decision tree, etc.
[15]	2021	Channel-based	Deep neural network
[16]	2021	Channel-based	Semi-supervised SVM
[17]	2021	Prior-knowledge-based	Bayesian filter
[19]	2021	Prior-knowledge-based	Kalman filter
[1]	2020	Map-based	Least squares
[20]	2020	Channel-based	Long short-term memory
[7]	2020	Map-based	Particle filter
[18]	2020	Others[1]	Kalman filter
[10]	2019	Channel-based	Fuzzy set theory
This study		Map-based	Gray wolf optimization

[1] Both UWB and inertial navigation systems were applied.

II. RELATED WORKS

To tackle the UWB NLOS mitigation challenges, the key is to characterize and mitigate the effect of NLOS obstacles on the UWB signal propagation path. Recent studies in the literature can be classified into four categories: 1) channel-based methods [14], [15], [16], 2) prior-knowledge-based methods [17], 3) map-based methods [1], [7], and 4) others [18]. The method proposed in this study is a map-based method. Table I summarizes the notable UWB NLOS mitigation research over the past three years.

The channel-based methods rely on the fact that UWB channel statistics [10] or diagnosis information [14] changes as UWB signals penetrate through obstacles. Researchers tried to build a relationship (or regression model) between the channel information and NLOS errors in advance, and used the relationship and field channel data to estimate the NLOS errors, and then mitigated the errors in UWB ranging or positioning. For example, Yu et al. [10] proposed a fuzzy comprehensive evaluation method to classify UWB channels into multiple cases, such as LOS and penetrating concrete walls, and estimated the NLOS errors based on the different cases. Similarly, machine learning algorithms, such as deep neural networks, have been used to establish relationships between the channel information and through-wall NLOS errors [15]. However, the relationships are unstable and not easy to build because extensive measurement campaigns are required on site [1]. Furthermore, not all the UWB sensors have access to channel information [17].

Prior knowledge includes thresholds or probability density functions of the ranging or positioning errors [10], [17]. Based on the modeled prior knowledge, Bayesian filters [17], such as Kalman filter [18] and particle filter [9], are often used to mitigate the NLOS errors. However, the prior knowledge is only applicable to some specific scenarios [10] and/or additional acceleration sensors [17]. For example, Barbieri et al. developed a Bayesian filtering method with a prior probability density function of the NLOS errors and assumed that the velocity vector of the tag was known [17].

Authorized licensed use limited to: Missouri University of Science and Technology. Downloaded on August 16,2023 at 18:44:54 UTC from IEEE Xplore. Restrictions apply.

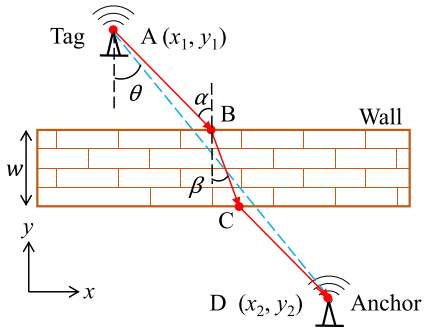

Fig. 1. Through-wall UWB wave propagation.

For a relatively static indoor environment, map-based methods can leverage through-wall error models to reduce each NLOS ranging error. Silva and Hancke [1] developed a through-wall NLOS error model using regression analysis. Ngo et al. [12] derived the theoretical bounds of through-wall NLOS errors. In the work of Silva and Hancke [1] and Ngo et al. [12], the relative permittivities of different walls were assumed to be the same in the various positioning scenarios for simplicity. Djaja-Josko and Kolakowski [11] assumed the through-wall UWB waves were perpendicular to walls. However, in a more realistic scenario, a UWB ranging process could involve different incidence angles and multiple walls with different thicknesses and materials. Furthermore, with a 1-m NLOS ranging error, the tag may be localized in different rooms, resulting in distinct through-wall error estimates. For example, Silva and Hancke [1] used a trilateration algorithm to obtain a preliminary position of the UWB tag and they assumed that the position accuracy was sufficient to select the error model. However, when the UWB tag was near the edge of a room, the preliminary estimate was likely to be in a different room. Because the error models were clearly different for different rooms, they may incorrectly calculate the ranging errors based on the preliminary tag position. In addition, UWB error maps can help to improve the positioning accuracy [7]. However, this type of method requires intensive grid measurements [17].

Based on the above review, each type of method has its own advantages and disadvantages. A new through-multiple-wall UWB indoor localization algorithm is required with more realistic error models, less time-consuming on-site measurements, and independent of preliminary estimated position.

III. UWB Through-Wall Ranging

A. UWB Through-Wall Propagation

As UWB signals propagate through a wall, as shown in Fig. 1, the electromagnetic propagation medium first changes from air to the wall and then back to air again, and the signals are reflected, refracted, scattered, and diffracted, resulting in attenuation and waveform distortion of the UWB signal [3], [21]. The UWB signal attenuation is similar to what happens when a narrowband signal propagates through a wall. The waveform distortion is caused by the dispersion of the complex permittivities of indoor building materials. Both the attenuation and distortion reduce the signal-to-noise ratio, resulting in a reduced range for the UWB [21]. While UWB ranging signals cannot penetrate very thick walls, they can pass through most of the common building walls [1].

During the propagation of the penetrated UWB signals inside a wall, both the propagation path and speed of the signals are changed by the wall [3]. Compared with multipath propagation and door/window obstruction, the through-wall NLOS cases are the main error source for UWB positioning systems [22], which is the focus of this article.

B. UWB Through-Wall Ranging Error

Several assumptions were made in this study: At least three UWB signals are still strong enough to range after penetrating walls; the relative permittivities of the air on both sides of the wall are the same and equal to one; the wall thickness can be obtained by maps or field measurements. Based on these assumptions, from the perspective of the TOA of a UWB signal, UWB through-wall ranging errors can be explained as follows. To illustrate the error more clearly, we select a wall, UWB tag, and UWB anchor as an example. In the schematic shown in Fig. 1, UWB signals propagate from point $A\ (x_1, y_1)$ through the wall to point $D\ (x_2, y_2)$. Point B is the incident point, α is the incidence angle, β is the refraction angle, and θ is the angle between the two UWB nodes and the wall.

The propagation path of the UWB signal from point A to point D is realized in several different segments, i.e., from point A to point B, then to point C, and finally to point D. The relationship between the incidence angle and refraction angle is given by Snell's law [12], which is the basic technical support of this study

$$\frac{\sin\alpha}{\sin\beta} \approx \sqrt{\varepsilon_r} \tag{1}$$

where ε_r is the relative permittivity of the wall. In general indoor positioning scenarios, $\varepsilon_r > 1$ and $0 \le \alpha < \frac{\pi}{2}$ [1]. The propagation speed of UWB waves in the air is approximately the speed of light c while the speed in a wall is given by [1]

$$v_w \approx \frac{c}{\sqrt{\varepsilon_r}}. \tag{2}$$

Therefore, the actual time-of-arrival (TOA) is as follows:

$$t = \frac{d_{AB}}{c} + \frac{d_{BC}\sqrt{\varepsilon_r}}{c} + \frac{d_{CD}}{c} \tag{3}$$

where d_{AB}, d_{BC}, and d_{CD} are the Euclidean distances between the corresponding points.

However, the TOA-based UWB range between point A and point D is determined by multiplying (3) by c [1], [12]

$$\begin{aligned} \hat{d}_{AD} &= ct \\ &= d_{AB} + d_{BC}\sqrt{\varepsilon_r} + d_{CD} \end{aligned}. \tag{4}$$

It is known that $d_{AB} + d_{BC} + d_{CD} \ge d_{AD}$, where d_{AD} is the Euclidean distance between point A and point D, and $\varepsilon_r > 1$. These two factors cause the TOA-based UWB through-wall

Authorized licensed use limited to: Missouri University of Science and Technology. Downloaded on August 16,2023 at 18:44:54 UTC from IEEE Xplore. Restrictions apply.

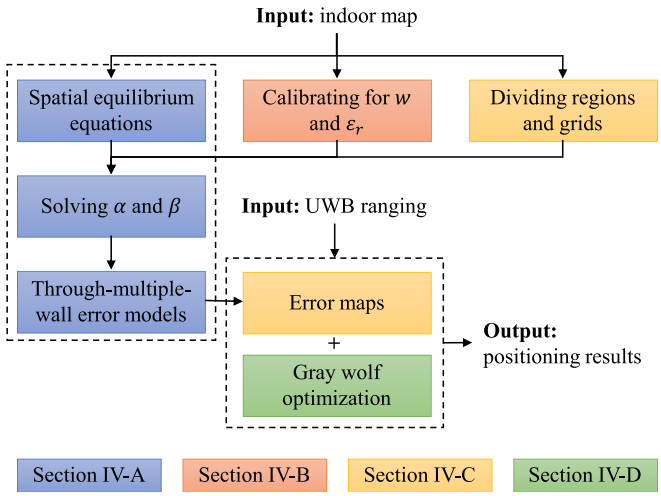

Fig. 2. Proposed NLOS mitigation method for UWB localization with multiple walls.

ranging results to be inaccurate. The ranging error of the TOA-based method in this situation is calculated as follows:

$$\begin{aligned} e &= \hat{d}_{AD} - d_{AD} \\ &= \frac{|y_1 - y_2| - w}{\cos\alpha} + \frac{w}{\cos\beta}\sqrt{\varepsilon_r} - d_{AD} \end{aligned} \tag{5}$$

where w is the thickness of the wall, and $|\cdot|$ denotes the absolute value. However, it is difficult to calculate the NLOS errors using (5) since the refraction angle β is unknown, especially when UWB waves travel through multiple walls with different intersection angles [12].

IV. Proposed Method

Fig. 2 shows the block diagram of our proposed method for NLOS mitigation. In Section IV-A, we present a numerical solution with spatial geometric equilibrium equations for the through-multiple-wall ranging error model. After using the calibration process presented in Section IV-B and dividing the map into regions and grids, the numerical solution is then used to calculate error maps for the entire positioning system in Section IV-C. Finally, the calculated error maps are combined with a GWO algorithm to mitigate the positioning error in Section IV-D.

A. Solving Ranging Errors Using Spatial Equilibrium Equations

As shown in Fig. 1, the following geometric relationships exist in the *X*- and *Y*-directions:

$$(d_{AB} + d_{CD})\sin\alpha + w\tan\beta = |x_1 - x_2|, \tag{6}$$

$$(d_{AB} + d_{CD})\cos\alpha + w = |y_1 - y_2|. \tag{7}$$

We define $m = d_{AB} + d_{CD}$. Therefore, (1), (6), and (7) can form a system of three-variable trigonometric equations:

$$\boldsymbol{F}(m,\alpha,\beta) = \begin{cases} f_1 = m\sin\alpha + w\tan\beta - |x_1 - x_2| \\ f_2 = m\cos\alpha + w - |y_1 - y_2| \\ f_3 = \frac{\sin\alpha}{\sin\beta} - \sqrt{\varepsilon_r} \end{cases} = 0 \tag{8}$$

where m, α, and β are the three unknown values. Equation (8) contains three unknown variables with four degrees and does not have a closed solution.

As classical optimization methods, gradient descent and Gauss–Newton algorithms can solve sums of squares of nonlinear functions, and thus solve nonlinear equations, such as (8). The Levenberg–Marquardt algorithm combines the gradient descent and Gauss–Newton algorithms by using a damping parameter [23]. During the iterative update, a large damping parameter will make the Levenberg–Marquardt algorithm close to the gradient descent algorithm, and a small damping parameter will make the algorithm close to the Gauss–Newton algorithm. In detail, the trial step Δ at each iteration is calculated as follows:

$$\Delta = -(\boldsymbol{J}^T\boldsymbol{J} + \lambda\boldsymbol{I})^{-1}\boldsymbol{J}^T\boldsymbol{F} \tag{9}$$

where λ is the damping parameter that is updated from iteration to iteration, $\boldsymbol{I}$ is the identity matrix, and $\boldsymbol{J}$ is the Jacobian matrix of $\boldsymbol{F}(m,\alpha,\beta)$. In this case

$$\begin{aligned} \boldsymbol{J} &= \begin{bmatrix} \frac{\partial f_1}{\partial m} & \frac{\partial f_1}{\partial \alpha} & \frac{\partial f_1}{\partial \beta} \\ \frac{\partial f_2}{\partial m} & \frac{\partial f_2}{\partial \alpha} & \frac{\partial f_2}{\partial \beta} \\ \frac{\partial f_3}{\partial m} & \frac{\partial f_3}{\partial \alpha} & \frac{\partial f_3}{\partial \beta} \end{bmatrix} \\ &= \begin{bmatrix} \sin\alpha & m\cos\alpha & \frac{w}{\cos^2\beta} \\ \cos\alpha & -m\sin\alpha & 0 \\ 0 & \frac{\cos\alpha}{\sin\beta} & -\frac{\sin\alpha\cos\beta}{\sin^2\beta} \end{bmatrix}. \end{aligned} \tag{10}$$

In addition, a well-known library in Python, "scipy," provides the Levenberg–Marquardt algorithm. This method requires an initial estimate of the unknown parameters (m_0, α_0, and β_0). We selected the following initial estimates:

$$m_0 = d_{AD} - w \tag{11}$$

$$\alpha_0 = \beta_0 = \arctan\left(\frac{|x_1 - x_2|}{|y_1 - y_2|}\right). \tag{12}$$

As shown in Fig. 3, UWB waves ranging through two walls, including parallel and perpendicular walls, are more complex. The proposed spatial geometric equilibrium equations are similar and can also determine the through-multiwall ranging errors in both cases. The following geometric relationships can be built in the *X*- and *Y*-directions for each scenario in Fig. 3. We set $m' = d_{AB} + d_{CD} + d_{EF}$.

For parallel walls, a system of four-variable trigonometric equations can be obtained as follows:

$$\boldsymbol{F}_{\parallel}(m,'\alpha,\beta_1,\beta_2) = \begin{cases} f_1 = m'\sin\alpha + w_1\tan\beta_1 \\ \quad +w_2\tan\beta_2 - |x_1 - x_2| \\ f_2 = m'\cos\alpha + w_1 + w_2 \\ \quad -|y_1 - y_2| \\ f_3 = \frac{\sin\alpha}{\sin\beta_1} - \sqrt{\varepsilon_{r1}} \\ f_4 = \frac{\sin\alpha}{\sin\beta_2} - \sqrt{\varepsilon_{r2}} \end{cases} = 0. \tag{13}$$

Authorized licensed use limited to: Missouri University of Science and Technology. Downloaded on August 16,2023 at 18:44:54 UTC from IEEE Xplore. Restrictions apply.

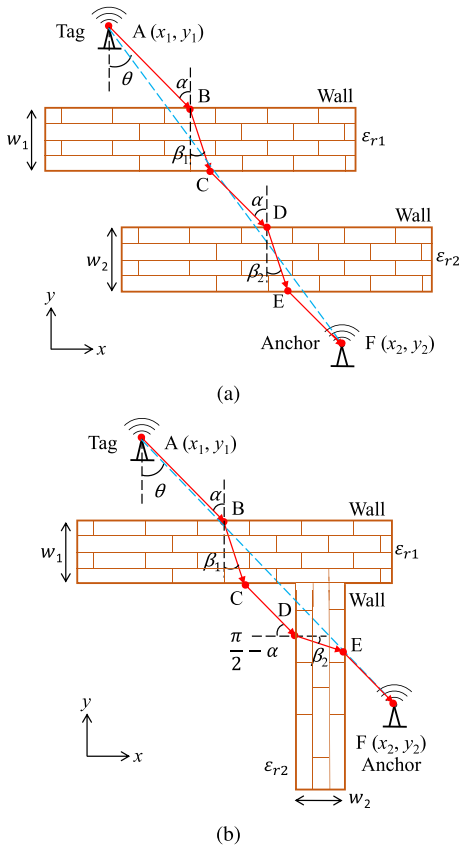

Fig. 3. More complex scenarios of UWB waves ranging through two walls: (a) parallel walls and (b) perpendicular walls. w_1 and w_2 denote the thicknesses of the two walls, respectively, ε_{r1} and ε_{r2} denote the relative permittivities of the two walls, respectively, and β_1 and β_2 are the first and the second refraction angles, respectively.

For perpendicular walls, a system of four-variable quadratic equations can be given as follows:

$$\boldsymbol{F}_{\perp}(m,' \alpha, \beta_1, \beta_2) = \begin{cases} f_1 = m'\sin\alpha + w_1\tan\beta_1 \\ \quad +w_2 - |x_1 - x_2| \\ f_2 = m'\cos\alpha + w_1 \\ \quad +w_2\tan\beta_2 - |y_1 - y_2| \\ f_3 = \frac{\sin\alpha}{\sin\beta_1} - \sqrt{\varepsilon_{r1}} \\ f_4 = \frac{\sin(\frac{\pi}{2}-\alpha)}{\sin\beta_2} - \sqrt{\varepsilon_{r2}} \end{cases} = 0. \quad (14)$$

Based on these equations, we can use the Levenberg–Marquardt algorithm to solve for the four unknown values, m', α, β_1, and β_2. The through-wall ranging errors in the two scenarios shown in Fig. 3 can be calculated respectively using the following equations:

$$e_{\parallel} = \frac{|y_1 - y_2| - w_1 - w_2}{\cos\alpha} + \frac{w_1}{\cos\beta_1}\sqrt{\varepsilon_{r1}} + \frac{w_2}{\cos\beta_2}\sqrt{\varepsilon_{r2}} - d_{AF} \quad (15)$$

$$e_{\perp} = \frac{|y_1 - y_2| - w_1 - w_2\tan\beta_2}{\cos\alpha} + \frac{w_1}{\cos\beta_1}\sqrt{\varepsilon_{r1}} + \frac{w_2}{\cos\beta_2}\sqrt{\varepsilon_{r2}} - d_{AF}. \quad (16)$$

In addition, this method can determine through-wall NLOS errors in arbitrary scenarios if we know the coordinates of the UWB nodes and walls as well as the properties of the walls.

Remark 1: This method is based on the properties of the wall (i.e., the thickness w and relative permittivity ε_r) and the position coordinates of the two UWB nodes are known.

To obtain the properties of the wall, a calibration process is proposed in Section IV-B. Obtaining the location coordinates of the UWB tag is a positioning problem, which is the purpose of this article and is addressed in Sections IV-C and IV-D.

B. Calibrating Parameters

Most commercial venues typically have detailed floor plans available [1]. The wall thickness w can be extracted from indoor maps. In addition, when deploying UWB anchors to predefined locations, we can measure the wall thickness simultaneously. However, the relative permittivity ε_r is difficult to determine because walls are nonhomogeneous and their materials are hard to determine [3]. Here, a calibration process is used to approximate the relative permittivity.

During the calibration process, two UWB nodes are placed on opposite sides of each wall, with their connecting line perpendicular to the wall. The distance between each UWB node and the wall is 50–200 cm, depending on the site conditions. There should be no obstacle other than the wall between the two UWB nodes. The true distance d_w between the two UWB nodes is first measured using a laser rangefinder or tape measure. A two-way time-of-flight method [7] is then adopted to collect the UWB ranging results using both UWB nodes. The relative permittivity of the wall can be approximated using [1], [3]:

$$\varepsilon_r \approx \left(\frac{\hat{d_w} - d_w}{w} + 1\right)^2 \quad (17)$$

where $\hat{d_w}$ denotes the UWB ranging result through the wall. The calibration requires W measurements, where W denotes the number of interior walls in the positioning system. The calibration workload is acceptable since it runs concurrently with the deployment of UWB anchors.

Remark 2: The relative permittivity of the wall obtained by calibration is subject to error, but this result can provide a basis for the subsequent calculations.

C. Calculating Error Maps

We consider localization in a two-dimensional indoor map $\mathcal{U} \subset \mathbb{R}^2$, where $\mathbb{R}$ denotes the set of real numbers. Fig. 4 shows an indoor positioning scenario with $W = 3$ interior walls, some exterior walls, and one UWB anchor. Here, we ignore the presence of the doors.

With the anchor as the end point, a number of rays are drawn through each wall's connection points, including end points and intersections. The rays and the walls divide the positioning plane into several minimum division units, such as $\mathcal{U}_{1,1}$ and $\mathcal{U}_{1,2}$, as shown in Fig. 4(a). If two line segments are drawn from the anchor to any point in the two adjacent minimum division units, and the number and order of the walls crossed by the two line

Authorized licensed use limited to: Missouri University of Science and Technology. Downloaded on August 16,2023 at 18:44:54 UTC from IEEE Xplore. Restrictions apply.

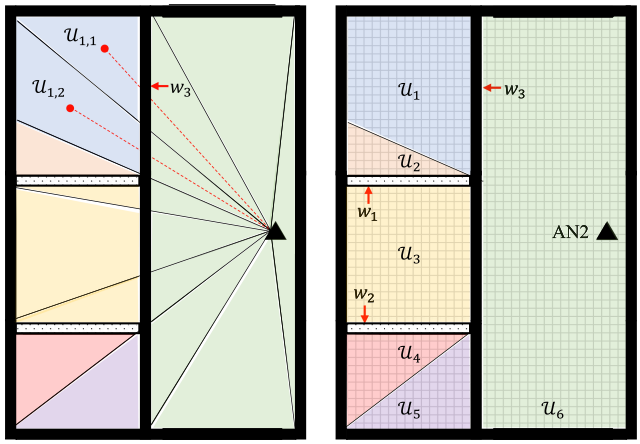

Fig. 4. Error map of the positioning system for Anchor 2: (a) segmentation process, where black lines denote the drawn rays and red dotted lines denote the example line segments; (b) segmentation results, where different color blocks denote different subareas.

segments are the same, then the two adjacent minimum division units belong to the same subarea. For example, in Fig. 4(a), two points are selected in the adjacent minimum division units $\mathcal{U}_{1,1}$ and $\mathcal{U}_{1,2}$, and the dotted red lines are drawn from the two points to the anchor, both the red line segments only pass through wall w_3. Therefore, the two adjacent minimum division units $\mathcal{U}_{1,1}$ and $\mathcal{U}_{1,2}$ belong to the same subarea $\mathcal{U}_1$.

The final division results are shown in Fig. 4(b). Depending on the combination of different walls, for each UWB anchor, the entire positioning area $\mathcal{U}$ can be divided into up to $\sum_{w=0}^{W} \mathrm{C}_W^w$ subareas. These subareas correspond to different through-wall cases. For example, the subarea $\mathcal{U}_4$ indicates that when the tag is in this subarea, the ranging between the tag and the anchor will be through the walls w_2 and w_3.

Next, the whole map can be divided into grids, each with a size of 10×10 cm. The UWB tag is placed in the center of each grid, at which point the position coordinates of the UWB tag and anchor and the wall properties (i.e., thickness and relative permittivity) are known. Therefore, the through-wall ranging error between the UWB tag and anchor can be determined by the method proposed in Section IV-A. Different subareas require different calculation equations. For example, (16) is required when the tag is in the $\mathcal{U}_4$ subarea.

The calculated ranging error between the tag in each grid and the ith anchor can be saved in a matrix as an offline error map

$$\boldsymbol{E}_i = \begin{bmatrix} e_{i,(1,1)} & e_{i,(1,2)} & \cdots & e_{i,(1,Y)} \\ e_{i,(2,1)} & e_{i,(2,2)} & \cdots & e_{i,(2,Y)} \\ \vdots & \vdots & \ddots & \vdots \\ e_{i,(X,1)} & e_{i,(X,2)} & \cdots & e_{i,(X,Y)} \end{bmatrix} \tag{18}$$

where X and Y denote the maximum number of grid elements in two directions.

Remark 3: The proposed error map is calculated based on the proposed error model and a simple calibration procedure, which, unlike the fingerprint method [7], does not require a large measurement effort.

D. Positioning Tags Using GWO Algorithm

We propose an error-map-based GWO algorithm for positioning tags in a two-dimensional through-wall scenario. The GWO algorithm is a metaheuristic algorithm with high local optima avoidance and computational speed [24]. The error-map-based GWO method is suitable for all types of distance-based localization questions. The main steps are summarized in Algorithm 1 as follows.

Step 1: Definition and initialization. There are $N \geq 3$ anchors and one tag in the positioning system. We define $\boldsymbol{x}_i = [x_i\ y_i]^T \subset \mathcal{U}$ as the position of the ith UWB anchor. In this scenario, based on a two-way time-of-flight method [7], UWB ranging can be used to measure the distances between N anchors and the tag. The corresponding measured ranges are denoted by $\hat{\boldsymbol{d}} = [\hat{d}_1\ \hat{d}_2\ \ldots\ \hat{d}_N]^T$. In addition, we define T as the maximum number of iterations and initialize $t = 0$ as the current number of iterations ($0 \leq t < T$). The positions $\boldsymbol{x}_k = [x_k\ y_k]^T \subset \mathcal{U}$ are initialized randomly, denoting the position of the kth wolf, $k \in \{1, 2, \ldots, K\}$, and K denotes the number of wolves.

Step 2: Calculating fitness. The fitness of the kth wolf is calculated as follows:

$$\tilde{d}_{i,\boldsymbol{x}_k} = \hat{d}_i - e_{i,\boldsymbol{x}_k} \tag{19}$$

$$f_{\boldsymbol{x}_k} = \sum_{i=1}^{N} |d_{i,\boldsymbol{x}_k} - \tilde{d}_{i,\boldsymbol{x}_k}| \tag{20}$$

where $d_{i,\boldsymbol{x}_k}$ and $\tilde{d}_{i,\boldsymbol{x}_k}$ denote the true Euclidean distance and the mitigated distance between the ith anchor and the kth wolf, respectively, $e_{i,\boldsymbol{x}_k}$ can be read from (18), and $f_{\boldsymbol{x}_k}$ denotes the fitness of the kth wolf.

Step 3: Sorting fitness. The calculated fitness values are sorted, the smallest three fitness values are selected, and their corresponding positions are labeled as $\boldsymbol{x}_a$, $\boldsymbol{x}_b$, and $\boldsymbol{x}_c$.

Step 4: Updating positions. The positions $\boldsymbol{x}_k$ are updated using the following equations [24]:

$$\begin{cases} \boldsymbol{D}_{a,\boldsymbol{x}_k} = |2\boldsymbol{r}_1 \cdot \boldsymbol{x}_a - \boldsymbol{x}_k| \\ \boldsymbol{D}_{b,\boldsymbol{x}_k} = |2\boldsymbol{r}_2 \cdot \boldsymbol{x}_b - \boldsymbol{x}_k| \\ \boldsymbol{D}_{c,\boldsymbol{x}_k} = |2\boldsymbol{r}_3 \cdot \boldsymbol{x}_c - \boldsymbol{x}_k| \end{cases} \tag{21}$$

$$\begin{cases} \boldsymbol{x}_{k1} = \boldsymbol{x}_a - (2 - \frac{2t}{T}) \cdot (2\boldsymbol{r}_4 - 1) \cdot \boldsymbol{D}_{a,\boldsymbol{x}_k} \\ \boldsymbol{x}_{k2} = \boldsymbol{x}_b - (2 - \frac{2t}{T}) \cdot (2\boldsymbol{r}_5 - 1) \cdot \boldsymbol{D}_{b,\boldsymbol{x}_k} \\ \boldsymbol{x}_{k3} = \boldsymbol{x}_c - (2 - \frac{2t}{T}) \cdot (2\boldsymbol{r}_6 - 1) \cdot \boldsymbol{D}_{c,\boldsymbol{x}_k} \end{cases} \tag{22}$$

where $\{\boldsymbol{r}_1, \boldsymbol{r}_2, ..., \boldsymbol{r}_6\}$ are random vectors in [0,1]. Then

$$\boldsymbol{x}_k(t+1) = \frac{\boldsymbol{x}_{k1} + \boldsymbol{x}_{k2} + \boldsymbol{x}_{k3}}{3} \tag{23}$$

where $\boldsymbol{x}_k(t+1)$ denotes the position of the kth wolf in the $(t+1)$th iteration. After all positions of the K wolves are updated, one iteration is completed, and we set $t = t + 1$. Then, steps 2–4 are repeated until $t \geq T$.

Step 5: Output. After T iterations, the location with the best fitness is the final estimated location of the UWB tag.

Authorized licensed use limited to: Missouri University of Science and Technology. Downloaded on August 16,2023 at 18:44:54 UTC from IEEE Xplore. Restrictions apply.

Algorithm 1: UWB Through-Multi-Wall Positioning Algorithm.

Input: Locations of the UWB anchors $\boldsymbol{x}_i$; measured ranges $\hat{\boldsymbol{d}}$; error maps $\boldsymbol{E}_i$; maximum number of iterations T; the number of wolves K.

Output: Estimated location of the UWB tag.

1: *Initialization:* Set $t = 0$. Randomly initialize $\boldsymbol{x}_k = [x_k\ y_k]^T \subset \mathcal{U}$.
2: **for** $t = 0$ to T **do**
3: Calculate the fitness for all K wolves using (19) and (20).
4: Sort the K fitness values.
5: Set the positions with the smallest three fitness values to $\boldsymbol{x}_a$, $\boldsymbol{x}_b$, and $\boldsymbol{x}_c$.
6: Update the positions of the K wolves using (23).
7: **end for**
8: **return** $\boldsymbol{x}_a$

V. Evaluation and Analysis

A. Experimental Setup

1) Test Site: Two-dimensional experiments were performed in a factory with a hall and three rooms, as depicted in Fig. 5(a). Fig. 5(b) shows a photograph of the hall. The overall size of the factory was 14 × 20 m. The thicknesses of the three types of interior walls are denoted as w_1, w_2, and w_3.

2) Instruments: Four UWB nodes, based on a low-cost DW1000 module [9] with a 2-dB omnidirectional antenna, were used in the experiment, as shown in Fig. 5(b). Three of these nodes were used as anchors and one was used for the tag. All the UWB nodes were configured with the 3.993-GHz channel and a data rate of 110 kb/s. UWB ranging was conducted using a two-way time-of-flight method [7]. With this configuration, the frequency of ranging and positioning was 3.57 Hz [9]. Data collection and calculations were carried out on a PC with an i7-8565 U CPU with a frequency of 1.8 GHz and 8 GB of RAM.

The coordinates of the anchors were AN1 (3.30, 17.13), AN2 (12.82, 6.50), and AN3 (0.85, 0.30) (unit: m). The height of the UWB nodes was set to 2.5 m. A Mileseey rangefinder with an accuracy of 2 mm and a tape measure with an accuracy of 1 mm were used to find the true distances and positions.

3) Static Localization Experiment: Fig. 5(a) shows the layout of the static localization experiment. The design of the layout was limited by various goods stacked in the factory. The UWB tag was placed one by one at each of the 29 locations with known coordinates for ranging with the three UWB anchors. At each location, the measurement lasted for 2 min. With the positioning frequency of 3.57 Hz, the number of measurements at each location was approximately 420. Therefore, the total number of measurements was $29 \times 420 = 12,180$.

4) Continuous Localization Experiment: In the continuous localization experiments, a movable cart carried the UWB tag slowly (∼0.1 m/s) along predetermined trajectories in Room 2, Room 3, and Hall, and the lengths of the trajectories were

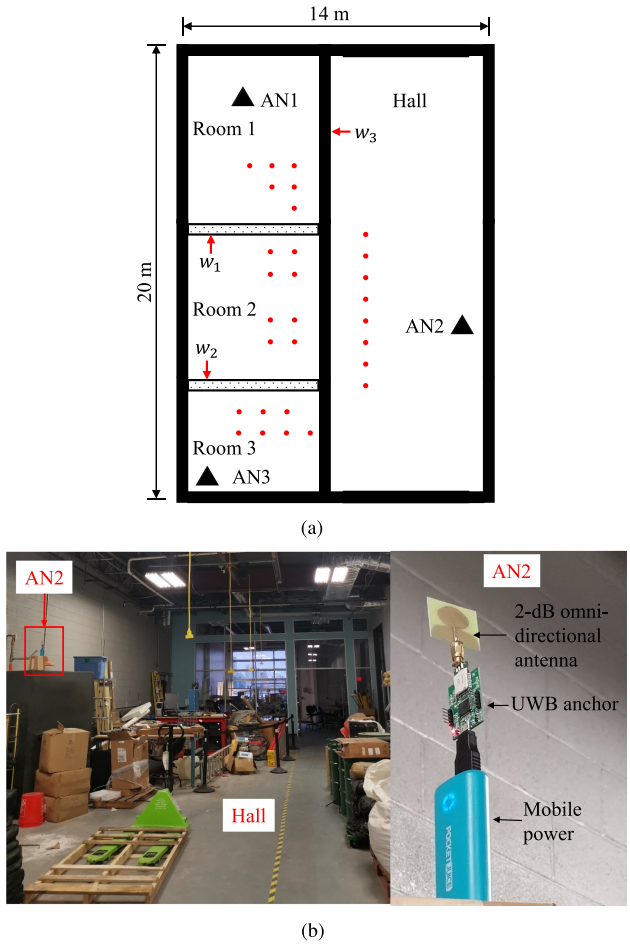

Fig. 5. Experimental site: (a) Layout and (b) photographs of the hall and the UWB anchor. "AN1," "AN2," and "AN3" denote the three UWB anchors. The 29 red dots denote the locations of the UWB tag.

655, 720, and 1150 cm, respectively. The total number of measurements was 1405. The reference trajectories included straight lines, L-shapes, and rectangles due to the constraints imposed by the locations of other objects in the rooms. The specific trajectories are given in Fig. 10.

5) Localization Algorithm Implementation: In the static and continuous experiments, three other map-based methods were also compared with the proposed algorithm. The first and second methods employed the traditional least-squares trilateration algorithm and they used the corrected ranging results based on the error models proposed in [11] and [12], named Model 1 and Model 2, respectively. The third algorithm was proposed in [1], named Model 3. In our algorithm, the anchor number N was equal to 3, wolf number K was set to 15, and iteration number T was set to 30.

B. Calibration and Calculated Error Map

From the layout of the factory, we obtained the thicknesses of the three walls, w_1, w_2, and w_3, which were 13, 13, and 20 cm, respectively. By applying the method in Section IV-C, the averages of the relative permittivities of walls w_1, w_2, and

Authorized licensed use limited to: Missouri University of Science and Technology. Downloaded on August 16,2023 at 18:44:54 UTC from IEEE Xplore. Restrictions apply.

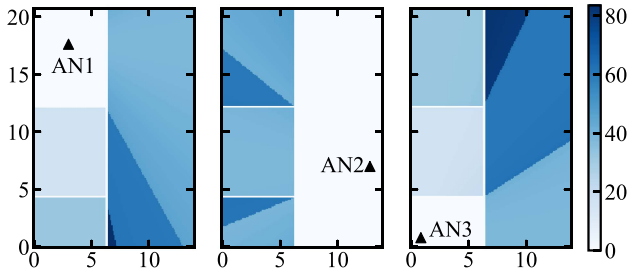

Fig. 6. Through-wall ranging error map for each anchor. From left to right are anchor 1, anchor 2, and anchor 3. Coordinate axes are in meters, and ranging errors are in centimeters.

TABLE II
RANGING ERRORS IN THE STATIC EXPERIMENT

Ranging with	Case	Original error (cm)		Mitigated error (cm)	
		Mean	STD	Mean	STD
AN1	LOS	45.84	28.38	16.49	14.83
	T1W	45.05	18.57	12.91	8.62
	T2W	61.57	20.56	19.29	12.57
	ALL	45.84	28.38	16.49	14.83
AN2	LOS	22.00	13.74	14.25	9.63
	T1W	43.70	12.05	12.53	8.29
	T2W	62.30	10.60	11.25	10.83
	ALL	38.93	21.52	12.13	8.44
AN3	LOS	20.81	15.46	14.54	7.01
	T1W	45.23	20.71	16.12	7.41
	T2W	50.51	9.10	10.88	6.89
	ALL	44.72	22.33	17.96	15.58
All	LOS	20.94	16.01	12.58	8.09
	T1W	44.52	16.79	13.59	8.31
	T2W	56.60	16.11	14.43	10.92
	ALL	43.16	24.46	15.53	13.57

[1] "LOS," "T1W," "T2W," and "ALL" denote the LOS case, through-one-wall NLOS case, through-two-wall NLOS case, and all the cases between the UWB anchor and tag.

w_3 were 4.97, 5.10, and 8.39, respectively, which required about 10 min in the field to determine. Then, the through-wall ranging error maps were calculated using the PC described in Section V-A as shown in Fig. 6. The calculation process took about 5 min in our office. When penetrating one wall, the average values of the measured and calculated errors were 44.52 and 31.28 cm, respectively, with a difference of 13.24 cm. When penetrating two walls, the mean measured error and calculated error were 56.60 and 45.35 cm, respectively, with a difference of 11.25 cm.

C. Static Experiment Results

1) Ranging Performance: The ranging performance was evaluated based on the absolute ranging errors, including the original measured and mitigated ranging errors. The evaluation metrics included the mean and standard deviations (STDs). Table II shows the ranging performance in the static experiment. The mean original ranging errors between the UWB tag and the anchors AN1, AN2, and AN3 were 45.84, 38.93, and 44.72 cm, respectively, and the overall mean ranging error was 43.16 cm. As a comparison, the proposed method effectively mitigated the ranging error. When ranging with anchors AN1, AN2, and AN3, the average mitigated ranging errors dropped

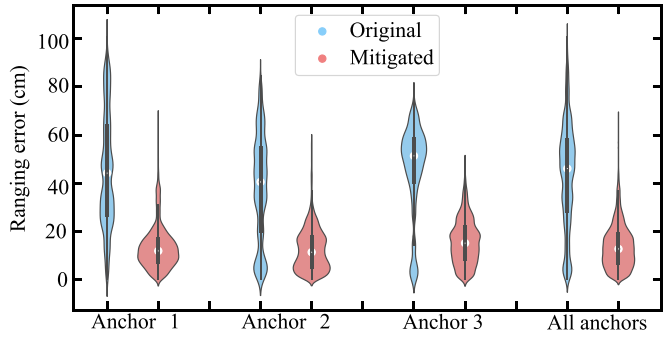

Fig. 7. Comparison of ranging errors in static experiments.

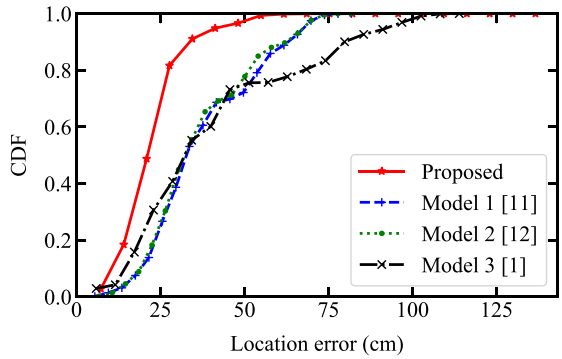

Fig. 8. CDF of the location errors in static experiments.

dramatically to 16.49, 12.13, and 17.96 cm, respectively. The overall mean ranging error decreased to 15.53 cm. Similarly, the standard deviation of the ranging error was reduced from 24.26 to 13.57 cm. Considering the different number of walls penetrated, the proposed method can reduce the original range errors by 40%, 69%, and 75% for the LOS, through-one-wall, and through-two-wall cases, respectively.

Fig. 7 shows the violin charts [25] of the different ranging error distributions. The width of each violin chart denotes its probability density. Fig. 7 shows the blue charts were long and thin, whereas the red charts were short and wide. This means that the original ranging errors were dispersed with long-tail behaviors while most of the mitigated ranging errors were more concentrated and smaller.

2) Localization Performance: The localization performance was evaluated based on the positioning error, i.e., the Euclidean distance between the true and estimated positions of the UWB tag. The average, standard deviation, and root-mean-square error (RMSE) of the positioning errors were applied to represent the localization performance [1], [10].

Table III shows the statistics of the location errors. In all the rooms, the RMSEs of the Model 1, Model 2, and Model 3 algorithms were 28.72, 27.96, and 33.54 cm, respectively, while the RMSE of the proposed method was reduced to 16.99 cm. Overall, the proposed algorithm yielded small means, standard deviations, and RMSEs compared to other methods. The performance for single rooms is discussed in Section V-E1.

Authorized licensed use limited to: Missouri University of Science and Technology. Downloaded on August 16,2023 at 18:44:54 UTC from IEEE Xplore. Restrictions apply.

TABLE III
STATIC LOCATION ERRORS USING DIFFERENT ALGORITHMS (UNIT: CM)

Algorithm	Room 1			Room 2			Room 3			Hall			All rooms		
	Mean	STD	RMSE	Mean	STD	RMSE	Mean	STD	RMSE	Mean	STD	RMSE	Mean	STD	RMSE
Model 1 [11]	33.60	4.31	23.95	23.40	5.49	17.00	33.90	17.34	26.93	56.84	7.19	40.51	37.24	16.22	28.72
Model 2 [12]	32.01	4.37	22.85	23.05	5.66	16.78	33.99	17.10	26.91	54.73	8.11	39.12	36.26	15.77	27.96
Model 3 [1]	15.72	7.11	12.20	24.80	6.08	18.06	60.55	22.54	45.68	55.86	22.68	42.63	40.10	25.34	33.54
Proposed	15.88	8.86	12.86	20.57	5.14	14.99	25.09	11.06	19.92	24.54	9.94	18.72	21.98	9.70	16.99

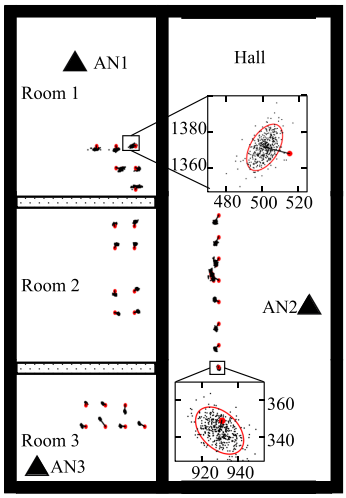

Fig. 9. Localization results using the proposed method in static experiments. The horizontal and vertical axes in the magnified figure are the *X* and *Y* axes, respectively. Coordinate axes are in centimeters.

Fig. 8 compares the cumulative distribution functions (CDFs) for the location errors obtained using different algorithms. The proposed method outperformed the other three map-based methods. For the proposed algorithm, 80% of the location errors were below 30 cm while those of other methods were larger, even up to 70 cm.

Fig. 9 shows the localization results for each UWB tag location, where red dots denote the true positions, black dots denote the estimated positions using our proposed method, and red ellipses denote the elliptical error probability at 95% confidence (EEP95) [17]. To emphasize the positioning errors, black lines were drawn between each true position and the mean location estimate. Most of the estimated locations were close to the real locations, and only several locations in Room 3 deviated from the real values.

D. Continuous Experiment Results

Fig. 10 shows the continuous localization results using the proposed algorithm. Due to the lack of real positions of the mobile UWB tag, measurable cross-track errors were used to evaluate the mobile positioning accuracy, i.e., the shortest distance from the estimated position to the reference trajectory [10]. The average cross-track error was 13.28 cm. Note that since the estimates did not always deviate vertically from the track, the cross-track errors served only as a reference.

Fig. 11 compares the localization performances using different algorithms in the continuous experiments. The proposed

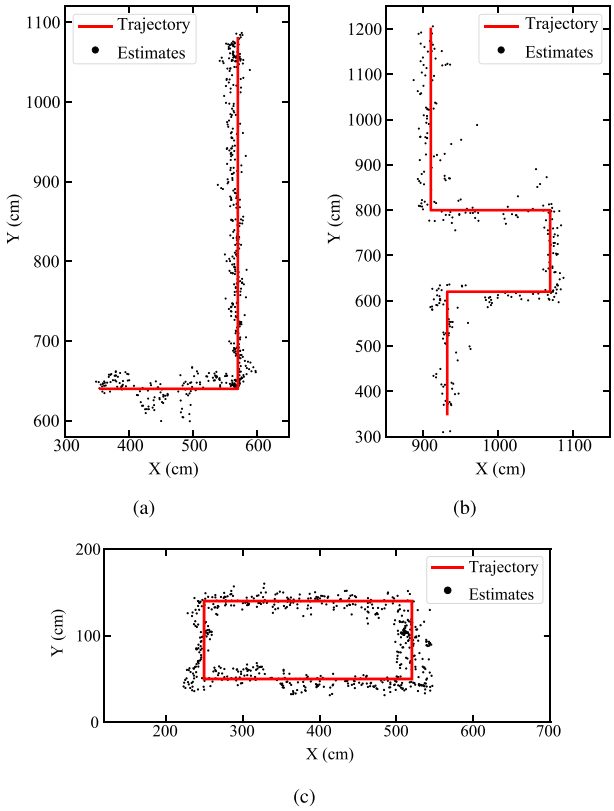

Fig. 10. Continuous localization results using the proposed method at different sites. (a) Room 2. (b) Hall. (c) Room 3.

method was better than the other three map-based methods. Over 80% of the cross-track errors using the proposed method were smaller than 25 cm while those of other three map-based methods were below 50–70 cm.

E. Discussion

1) Performance of Penetrating Multiple Walls: Fig. 12 compares the localization performances of the proposed method and other three map-based methods for different numbers of penetrating walls in static experiments. In Room 2, the UWB tag was separated from the three anchors by only one wall, and the localization errors of all the algorithms were relatively close to 16 cm. In the hall, two walls obstructed the UWB tag and the anchors AN1 and AN3. The RMSE of the proposed algorithm was 18.72 cm, which was clearly smaller than those of the other three map-based methods. Details can be found in Table III. The results showed that the proposed algorithm performed better in the multiple-wall scenarios.

Authorized licensed use limited to: Missouri University of Science and Technology. Downloaded on August 16,2023 at 18:44:54 UTC from IEEE Xplore. Restrictions apply.

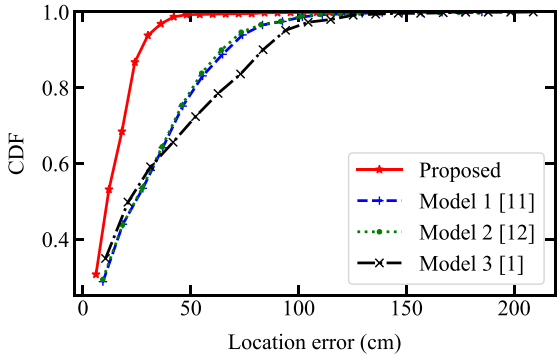

Fig. 11. CDF of the cross-track location errors in the continuous experiments.

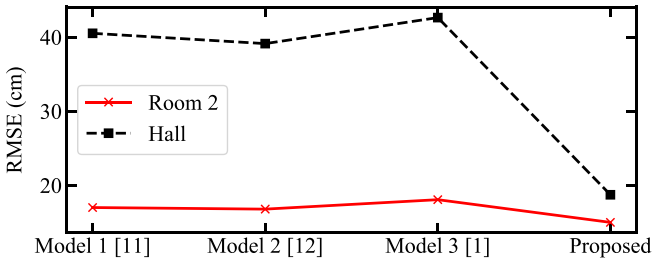

Fig. 12. Localization error with different numbers of wall penetrations.

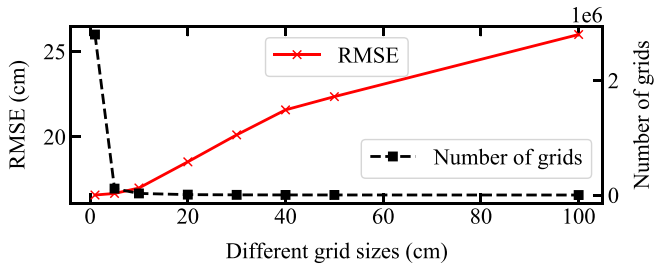

Fig. 13. Effect of using different grid sizes in the error maps.

2) Effect of Uneven Walls on Localization Accuracy: Since walls are nonhomogeneous and the relative permittivities of the walls must be approximated in the calibration process, it is necessary to discuss the effect of uneven walls on the performance of the proposed method. The calibrated relative permittivities were modified from −30% to 30% with a step size of 10% to calculate the locations of the UWB tag in the static experiments. The average localization error using the proposed method was slightly increased by 1.6 cm from 21.98 to 23.58 cm. As comparison, the error using Model 1 increased by 4.54 cm, whereas that using Model 2 was increased by 4.55 cm. As Model 3 did not use the relative permittivity, the results were unchanged. Even so, the accuracy using the proposed method was still the best. This means the acceptable variations in relative permittivity had little effect on the localization accuracy of the method.

3) Effect of Grid Size: Here, we set up eight different grid sizes, including 1×1, 5×5, 10×10, 20×20, 30×30, 40×40, 50×50, and 100×100 cm. Accordingly, we used these eight grid sizes to calculate eight error maps, which were used in the static experiments. Other experimental environments and conditions were unchanged. Fig. 13 shows the relationship between the grid size and the localization errors as well as the relationship between the grid size and the number of grid elements of the error maps. The RMSE of the proposed method increased as the grid became larger while the number of grid elements of the calculated error maps decreased rapidly. When the grid size was 10×10 cm, the RMSE of the proposed method was 16.99 cm and the number of grid elements of the error maps was 28 000, achieving a balance between the number of grid elements and the localization performance. In addition, we calculated the estimation rate of the localization system [6], which is related to the grid size. For the eight grid sizes, the estimation rates were 0.1%, 1.1%, 6.6%, 44.1%, 86.4%, 94.3%, 97.5%, and 100%, respectively. It is worth mentioning that the grid size did not affect the field workload using the proposed method. The grid size can be adjusted based on the hardware of the calculation platform.

4) Robustness: In the factory experiment, there were four rooms, three interior walls with different thicknesses and relative permittivities, and six types of penetration situations. To further verify the robustness, we conducted another UWB indoor localization experiment in a lounge and two restrooms with an overall size of 5.87×7 m. There were other two walls and three penetration cases. The experimental configurations were similar to those in the factory experiments. The positions of the anchors were AN1 (2.5, 0.35), AN2 (0.5, 6.5), and AN3 (5.37, 6.5) (unit: m). The height of the UWB anchors and tag was 1.26 m. There were two interior walls on the site. The thicknesses were 30 and 13 mm. The relative permittivities were calibrated as 7.75 and 5.30. The overall mean ranging error decreased from 43.63 to 11.28 cm with a mitigation rate of 74%. The RMSE of the proposed method was reduced to 16.14 cm.

5) Effect of Wall Materials: We have investigated common indoor walls, including concrete, wood, gypsum, and brick walls. First, we calibrated these walls using the proposed method in Section IV-B. Based on the calibration results, we calculated the UWB through-wall ranging errors, which was 33.34, 19.53, 15.48, and 7.14 cm for the different walls. Then, we moved the UWB nodes but ensured they passed through the same wall. The average measured through-wall ranging errors were 37.61, 23.39, 17.03, and 10.76 cm for the different walls, respectively. Correspondingly, the difference between the calculated and measured ranging errors were 4.27, 3.86, 1.55, and 3.62 cm, respectively. The calculated ranging errors were close to the measured ranging errors, demonstrating that the proposed method is competent for different types of walls. Benefiting from the on-site calibration, we do not need to be particularly concerned with the type of wall. It should be noted that the walls in this study are common indoor walls with materials and thicknesses that allow UWB wave penetration.

6) Effect of Doors and Windows: To investigate the effect of doors and windows, we conducted one through-door and one

Authorized licensed use limited to: Missouri University of Science and Technology. Downloaded on August 16,2023 at 18:44:54 UTC from IEEE Xplore. Restrictions apply.

TABLE IV
COMPARISON OF THIS WORK WITH OTHER UWB MAP-BASED METHODS

	[1]	[12]	[11]	Proposed method
Technology	UWB	UWB	UWB	UWB
RMSE (cm)	21–40	54	50[1]	17
Validation method	Both	Test	Test	Test
Test area (m × m)	6×12	24×17	14×8	20×14
Multiple walls	Yes	Yes	No	Yes
Calibration for walls	No	Yes	Yes	Yes
Assumption 1[2]	Yes	Yes	No	No
Assumption 2[3]	Yes	Yes	Yes	No

[1] RMSE is calculated using the data in reference [11].
[2] Assumed the relative permittivities of different walls were the same.
[3] Assumed that the walls penetrated by UWB signals were known.

TABLE V
COMPARISON OF THIS WORK WITH FINGERPRINT METHOD

	[2]	[26]	[6]	Proposed
Wireless signals	Wi-Fi	Wi-Fi	LoRa	UWB
Hardware cost	Low	Low	Moderate	High
Anchor number	3	9	4	3
Indoor size (m^2)	20×20	73×20	50×100	20×14
Grid size	4×4 m	0.8-m interval	3-m spaced hexagon	0.1×0.1 m
Measurement number	150	175	149	3
Error (m)	1.38	2.50	1.76	0.22

through-window UWB ranging experiments. The door is made of wood and is a common interior door. The window is mainly made of glass. There were two UWB nodes in the experiments, and their configuration was the same as the previous one. Here, we considered the door and window as a specific type of wall and calibrated the door and window. And, we calculated the UWB through-door and through-window ranging errors as 4.80 and 0.93 cm, respectively. Then, we moved the UWB nodes and measured the ranging errors, which were close to the calculated ranging errors. In addition, we counted the thickness of 10 common interior doors and windows. The thickness of common interior doors in offices is between 3 and 5 cm, and the thickness of common interior windows is generally less than 1 cm. The general penetration ranging error is less than 6 cm. Therefore, we can use our approach to calibrate doors or windows and then mitigate the ranging error to improve the accuracy of the positioning system, or we can directly treat the door or window as a LOS case to simplify the system.

F. Comparison With Other Studies

Table IV shows the comparisons of the results from the proposed and other map-based UWB positioning approaches. Silva and Hancke [1] did not require the calibration for walls, which is a great contribution. However, they assumed that the relative permittivities of multiple walls were identical and the walls being penetrated could be known. Ngo et al. [12] directly measured the UWB through-one-wall ranging error, which is one type of calibration. The measured through-one-wall ranging error was used to correct the UWB ranging results. And they made the same two assumptions. Djaja-Josko et al. [11] measured the delay of UWB signals introduced by different walls, which is another type of calibration. The delay multiplied by the propagation speed of the electromagnetic wave is the through-wall ranging errors. But they did not consider the multiwall scenarios and they also assumed that the walls penetrated by UWB signals are known. Based on these great works [1], [11], [12], our approach uses maps and calibration but does not rely on the two assumptions, and achieves a smaller RMSE than other methods.

Because the proposed method uses maps and calibration, which is similar to the fingerprint method, Table V compares the method with three excellent fingerprint methods. There were several experimental settings in [2]. Among them, a 20 × 20-m laboratory with 3 Wi-Fi nodes was divided into equal-sized grids with a size of 4 × 4 m. At each grid, six points were collected. A total of 150 on-site measurements were conducted to collect the received signal strength (RSS). The best average localization error was 1.38 m. Similarly, a 73 × 20-m indoor area surrounded by 9 Wi-Fi nodes was divided into 175 grid points with an interval of 0.8 m between adjoining points. The RMSE was 2.50 m [26]. Four long-range (LoRa) nodes were deployed in a 50 × 100-m indoor space [6]. The whole indoor space was divided into 3-m spaced hexagon girds. In the field, 149 measurements were conducted to build the fingerprint database. The average error distance was 1.76 m [6]. In the preparation of our experiment, we only conducted three on-site measurements to calibrate wall properties. Then, we calculated UWB ranging errors at each grid instead of measuring, meaning the grid number only increases the calculation instead of the measurement workload. Therefore, our approach using UWB technology has the advantage of high accuracy and low workload compared with the fingerprint methods using Wi-Fi and LoRa.

G. Limitations and Future Work

The study has some limitations that will be addressed in the future. Currently, only interior walls were investigated. The proposed method will be combined with other UWB NLOS mitigation methods to mitigate hybrid NLOS cases, such as NLOS errors induced by the simultaneous blocking of signals by walls, furniture, and human bodies. Furthermore, the proposed method assumes the UWB through-wall signals can function properly. We will combine this work with signal characteristics and coverage. In addition, we will verify the robustness or generality in more scenarios, and we will extend this work from localization to tracking by adding prediction methods, such as the Kalman filter.

VI. CONCLUSION

In this article, we present an NLOS mitigation method for UWB indoor positioning with multiple walls. Specifically, we develop spatial geometric equilibrium equations of UWB through-wall propagation to accurately model UWB through-multiwall ranging errors. Based on the modeled ranging errors, we calculate error maps without time-consuming field measurements. Finally, we propose a localization algorithm that incorporates the error map and GWO. The solution is effective

Authorized licensed use limited to: Missouri University of Science and Technology. Downloaded on August 16,2023 at 18:44:54 UTC from IEEE Xplore. Restrictions apply.

for realistic industrial environments with multiple walls and different relative permittivities. We conducted field experiments in different scenarios to evaluate the method. The RMSE of the proposed algorithm was 16.99 cm, which was 60% less than that without NLOS mitigation. The effects of penetrating different walls, inhomogeneity of the walls, and different grid sizes and robustness were discussed. The results showed the effectiveness of the proposed method in improving the location estimation performance in a multi-wall scenario. In the future, we will further consider hybrid NLOS scenarios and signal coverage, explore the robustness, and extend this work from positioning to track.

REFERENCES

[1] B. Silva and G. P. Hancke, "Ranging error mitigation for through-the-wall non-line-of-sight conditions," *IEEE Trans. Ind. Informat.*, vol. 16, no. 11, pp. 6903–6911, Nov. 2020.

[2] J. Luo, Z. Zhang, C. Wang, C. Liu, and D. Xiao, "Indoor multifloor localization method based on WiFi fingerprints and LDA," *IEEE Trans. Ind. Informat.*, vol. 15, no. 9, pp. 5225–5234, Sep. 2019.

[3] M. Dong, M. Miao, and Y. Qi, "Experimental study on ultra-wideband ranging through non-homogeneous walls," in *Proc. IEEE 13th Int. Symp. Antennas, Propag., EM Theory*, 2021, pp. 1–3.

[4] X. Yang, Z. Wu, and Q. Zhang, "Bluetooth indoor localization with Gaussian-Bernoulli restricted Boltzmann machine plus liquid state machine," *IEEE Trans. Instrum. Meas.*, vol. 71, Jan. 2022, Art. no. 1000208.

[5] A. A. N. Shirehjini and S. Shirmohammadi, "Improving accuracy and robustness in HF-RFID-based indoor positioning with Kalman filtering and Tukey smoothing," *IEEE Trans. Instrum. Meas.*, vol. 69, no. 11, pp. 9190–9202, Nov. 2020.

[6] H. Zhu et al., "Extreme RSS based indoor localization for LoRaWAN with boundary autocorrelation," *IEEE Trans. Ind. Informat.*, vol. 17, no. 7, pp. 4458–4468, Jul. 2021.

[7] X. Zhu, J. Yi, J. Cheng, and L. He, "Adapted error map based mobile robot UWB indoor positioning," *IEEE Trans. Instrum. Meas.*, vol. 69, no. 9, pp. 6336–6350, Sep. 2020.

[8] A. R. J. Ruiz and F. S. Granja, "Comparing Ubisense, BeSpoon, and DecaWave UWB location systems: Indoor performance analysis," *IEEE Trans. Instrum. Meas.*, vol. 66, no. 8, pp. 2106–2117, Aug. 2017.

[9] Q. Tian, I. Kevin, K. Wang, and Z. Salcic, "Human body shadowing effect on UWB-based ranging system for pedestrian tracking," *IEEE Trans. Instrum. Meas.*, vol. 68, no. 10, pp. 4028–4037, Oct. 2019.

[10] K. Yu, K. Wen, Y. Li, S. Zhang, and K. Zhang, "A novel NLOS mitigation algorithm for UWB localization in harsh indoor environments," *IEEE Trans. Veh. Technol.*, vol. 68, no. 1, pp. 686–699, Jan. 2019.

[11] V. Djaja-Josko and M. Kolakowski, "A new map based method for NLOS mitigation in the UWB indoor localization system," in *Proc. IEEE 25th Telecommun. Forum*, 2017, pp. 1–4.

[12] Q.-T. Ngo, P. Roussel, B. Denby, and G. Dreyfus, "Correcting non-line-of-sight path length estimation for ultra-wideband indoor localization," in *Proc. IEEE Int. Conf. Localization GNSS*, 2015, pp. 1–6.

[13] A. K. Singh, R. Pamula, and G. Srivastava, "An adaptive energy aware DTN-based communication layer for cyber-physical systems," *Sustain. Comput.: Inform. Syst.*, vol. 35, Sep. 2022, Art. no. 100657.

[14] A. G. Ferreira, D. Fernandes, S. Branco, A. P. Catarino, and J. L. Monteiro, "Feature selection for real-time NLOS identification and mitigation for body-mounted UWB transceivers," *IEEE Trans. Instrum. Meas.*, vol. 70, Apr. 2021, Art. no. 5502310.

[15] S. Angarano, V. Mazzia, F. Salvetti, G. Fantin, and M. Chiaberge, "Robust ultra-wideband range error mitigation with deep learning at the edge," *Eng. Appl. Artif. Intell.*, vol. 102, Jun. 2021, Art. no. 104278.

[16] T. Wang, K. Hu, Z. Li, K. Lin, J. Wang, and Y. Shen, "A semi-supervised learning approach for UWB ranging error mitigation," *IEEE Wireless Commun. Lett.*, vol. 10, no. 3, pp. 688–691, Mar. 2021.

[17] L. Barbieri, M. Brambilla, A. Trabattoni, S. Mervic, and M. Nicoli, "UWB localization in a smart factory: Augmentation methods and experimental assessment," *IEEE Trans. Instrum. Meas.*, vol. 70, Apr. 2021, Art. no. 2508218.

[18] D. Feng, C. Wang, C. He, Y. Zhuang, and X.-G. Xia, "Kalman-filter-based integration of IMU and UWB for high-accuracy indoor positioning and navigation," *IEEE Internet Things J.*, vol. 7, no. 4, pp. 3133–3146, Apr. 2020.

[19] B. Cao, S. Wang, S. Ge, and W. Liu, "Improving positioning accuracy of UWB in complicated underground NLOS scenario using calibration, VBUKF, and WCA," *IEEE Trans. Instrum. Meas.*, vol. 70, Jan. 2021, Art. no. 8501013.

[20] Y.-Y. Chen, S.-P. Huang, T.-W. Wu, W.-T. Tsai, C.-Y. Liou, and S.-G. Mao, "UWB system for indoor positioning and tracking with arbitrary target orientation, optimal anchor location, and adaptive NLOS mitigation," *IEEE Trans. Veh. Technol.*, vol. 69, no. 9, pp. 9304–9314, Sep. 2020.

[21] Z. Yun and M. F. Iskander, "UWB pulse propagation through complex walls in indoor wireless communications environments," in *Proc. IEEE Int. Conf. Wireless Netw., Commun., Mobile Comput.*, 2005, pp. 1358–1361.

[22] C. Chen, H. Ding, X. Huang, X. Li, and J. Yuan, "Through-wall localization with UWB sensor network," in *Proc. IEEE Int. Conf. Ultra-Wideband*, 2012, pp. 284–287.

[23] J. J. Moré, "The Levenberg-Marquardt algorithm: Implementation and theory," in *Numerical Analysis*. Berlin, Germany: Springer, 1978, pp. 105–116.

[24] S. Mirjalili, S. M. Mirjalili, and A. Lewis, "Grey wolf optimizer," *Adv. Eng. Softw.*, vol. 69, pp. 46–61, Mar. 2014.

[25] J. L. Hintze and R. D. Nelson, "Violin plots: A box plot-density trace synergism," *Amer. Statistician*, vol. 52, no. 2, pp. 181–184, 1998.

[26] X. Guo, N. R. Elikplim, N. Ansari, L. Li, and L. Wang, "Robust WiFi localization by fusing derivative fingerprints of RSS and multiple classifiers," *IEEE Trans. Ind. Informat.*, vol. 16, no. 5, pp. 3177–3186, May 2020.

Mengyao Dong (Graduate Student Member, IEEE) received the B.S. degree in information engineering in 2016 from Southwest Jiaotong University, Chengdu, China, where she is currently working toward the Ph.D. degree in information and communication engineering.

Her current research interests include indoor positioning and electromagnetic wave.

Yihong Qi (Senior Member, IEEE) received the Ph.D. degree in electronics from Xidian University, Xi'an, China, in 1989.

He is currently the President of General Test Systems, Inc., Shenzhen, China, the President of Link-E, Zhuhai, China, and the CTO of Pontosense, Toronto, ON, Canada. He is an Honorary Professor with Xidian University and Southwest Jiaotong University. He is also an Adjunct Professor with EMC Laboratory, Missouri University of Science and Technology, Rolla, MO, USA; Western University, London, ON, Canada; Hunan University, Changsha, China; Dalian Maritime University, Dalian, China, and Southwest University of Science and Technology, Mianyang, China. He is an inventor of more than 500 published and pending patents. From 1995 to 2010, he was with Research in Motion (Blackberry), Waterloo, ON, where he was the Director of Advanced Electromagnetic Research.

Dr. Qi was a Distinguished Lecturer of IEEE EMC Society and the founding Chairman of the IEEE EMC TC-12. He is recipient of an IEEE EMC Society Technical Achievement Award, CES Innovation Award 2019 and 2020, Network Product of the year in Award 2021, and Wellness Product of the Year Award 2022. He is an Associate Editor for the IEEE INTERNET OF THINGS JOURNAL and IEEE TRANSACTIONS ON ELECTROMAGNETIC COMPATIBILITY. He is a Fellow of the Canadian Academy of Engineering and a Fellow of the National Academy of Inventors.

Authorized licensed use limited to: Missouri University of Science and Technology. Downloaded on August 16,2023 at 18:44:54 UTC from IEEE Xplore. Restrictions apply.

Xianbin Wang (Fellow, IEEE) received the Ph.D. degree in electrical and computer engineering from the National University of Singapore, Singapore, in 2001.

He is currently a Professor and a Tier-1 Canada Research Chair with Western University, London, ON, Canada. Prior to joining Western, he was with Communications Research Centre Canada (CRC) as a Research Scientist/Senior Research Scientist between July 2002 and December 2007. From January 2001 to July 2002, he was a System Designer with STMicroelectronics. He has more than 500 highly cited journal and conference papers, in addition to 30 granted and pending patents and several standard contributions. His current research interests include 5G/6G technologies, Internet-of-Things, communications security, machine learning, and intelligent communications.

Dr. Wang is a Fellow of the Canadian Academy of Engineering, a Fellow of the Engineering Institute of Canada, and an IEEE Distinguished Lecturer. He has received many awards and recognitions, including Canada Research Chair, CRC President's Excellence Award, Canadian Federal Government Public Service Award, Ontario Early Researcher Award, and six IEEE Best Paper Awards. He currently serves/has served as an Editor-in-Chief, Associate Editor-in-Chief, Editor/Associate Editor for more than 10 journals. He was involved in many IEEE conferences including GLOBECOM, ICC, VTC, PIMRC, WCNC, CCECE, and CWIT, in different roles such as General Chair, Symposium Chair, Tutorial Instructor, Track Chair, Session Chair, TPC Co-Chair, and Keynote Speaker. He has been nominated as an IEEE Distinguished Lecturer several times during the last 10 years. He was the Chair of IEEE ComSoc Signal Processing and Computing for Communications (SPCC) Technical Committee between 2018 and 2021. He is currently the Chair of IEEE London Section.

Yiming Liu received the B.S. and M.S. degrees in industrial engineering in 2013 and 2016, respectively, from Southwest Jiaotong University, Chengdu, China, where he is currently working toward the Ph.D. degree in information and communication engineering.

His current research interests include indoor positioning and machine learning.

Authorized licensed use limited to: Missouri University of Science and Technology. Downloaded on August 16,2023 at 18:44:54 UTC from IEEE Xplore. Restrictions apply.